J. Fluid Mech. (1988), *vol.* 196, *pp.* 449–465
Printed in Great Britain

Viscoelastic inertial flow driven by an axisymmetric accelerated surface

By R. G. LARSON
AT & T Bell Laboratories, Murray Hill, NJ 07974, USA

(Received 17 July 1987 and in revised form 1 April 1988)

A similarity transform is used to analyse the flow of an upper-convected Maxwell fluid in an infinitely long cylinder whose surface has a velocity that increases in magnitude linearly with axial coordinate. Two types of problem are considered, the accelerated surface flow – when the surface velocity is outward towards the tube ends, and the decelerated surface flow – when it is inward. For the accelerated surface flow, the introduction of elasticity prevents the loss of similarity solution that occurs without elasticity at a Reynolds number (Re) of 10.25; with elasticity, solutions up to a Reynolds number of 95 were computed. As elasticity is introduced, normal stress gradients in an elastic boundary layer near the accelerated surface help offset inertially generated negative axial pressure gradients; with sufficient elasticity the turning point in the non-elastic solution family at $Re = 10.25$ disappears. For the decelerated surface flow, solutions could not be computed beyond a critical Re that depends on the level of elasticity considered, because at this critical Re, the axial velocity profile at the centreline becomes infinitely blunt.

1. Introduction

Multidimensional flows of viscoelastic fluids, with or without inertial effects, have proven exceedingly difficult to analyse, in general much more difficult than Newtonian inertial flows. This is in part because representations of viscoelasticity usually involve not just the inclusion of nonlinear terms in the momentum-balance equation, as is the case when one considers inertia, but either an additional set of partial differential equations that couple to each other and to the momentum-balance equation, or a history integral for the stress tensor, which, when substituted into the momentum-balance equation, produces difficult integro–differential equations. As a result, most investigators have resorted directly to finite-element or finite-difference techniques to obtain approximate solutions.

The most obvious implementations of these techniques, however, have failed to provide reliable answers outside the uninteresting regime in which the elastic effects are small and the flow is nearly that of a Newtonian liquid. Progress toward more robust numerical schemes has been hard-won and slow in coming. Therefore it is important that analytic solutions be found for non-trivial viscoelastic flows. Such solutions will assist both in the understanding of how elastic forces influence fluid motion and stress, and in the development of computational schemes better suited to the mathematical structure of such problems.

Until recently, the only analytic solutions for multidimensional viscoelastic flows were those obtained by perturbation techniques, valid when the velocities are small, or the fluid is nearly Newtonian. Solutions, even exact solutions, for fluids described as second order or third order, should be thought of as perturbation results, since

such fluid descriptions are obtained by truncating the retarded motion expansion, which is itself a perturbation expansion, valid only for slow and slowly varying flows.

Recently, however, similarity solutions have been discovered for certain axisymmetric and planar viscoelastic flows. Phan-Thien 1983(*a*, *b*) analysed the inertial and inertialess flows of upper-convected Maxwell and Oldroyd-B fluids between two rotating coaxial disks, using a similarity transform. He found that the inertialess flow of a Maxwell fluid between the disks becomes unstable at a Deborah number of 1.4. The Deborah number is a measure of the strength of the elastic compared to the viscous forces. A similarity transformation also allowed Menon *et al.* (1988) and Larson (1988) to study the flow of a Maxwell fluid in a porous cylinder. For a Maxwell fluid uniformly injected through the walls of the infinite cylinder they found a limit point or turning point at a Deborah number of around 0.07.

2. Problem definition

Here, we shall consider the inertial flow of a Maxwell fluid inside an infinite cylinder, when the magnitude of the axial velocity at the cylinder surface increases linearly with the axial coordinate; i.e.

$$v_z(1) = z; \quad v_r(1) = 0, \tag{1}$$

where r and z are the dimensionless axial and radial coordinates and v_z and v_r are the dimensionless axial and radial components of velocity; see figure 1. The cylinder has a dimensionless radius of unity. Brady & Acrivos (1981, 1982) and Durlofsky & Brady (1984), who considered this problem for a Newtonian fluid, were originally motivated by an interest in the flow inside a long cylindrical droplet whose surface is dragged by an exterior extensional flow field. This and the porous-tube problem are closely related. In fact, as shown by Brady & Acrivos (1981) and discussed below, from each solution for the accelerated surface flow, with the boundary conditions given above, a solution for uniform suction from a porous tube can be obtained. The boundary condition for uniform suction is

$$v_r(1) = 1. \tag{2}$$

Here the dimensionless radius of the porous tube is again unity. The boundary condition for uniform injection into a porous tube is given by

$$v_r(1) = -1. \tag{3}$$

Solutions for uniform injection can also be obtained from an accelerated surface problem, but with negative acceleration, corresponding to

$$v_z(1) = -z; \quad v_r(1) = 0. \tag{4}$$

It is difficult to imagine a physical system wherein the above boundary conditions could actually be achieved for a viscoelastic fluid. The choice of these boundary conditions is motivated by the existence of a similarity solution and hence the tractability of this problem, and the hope that the analysis of tractable viscoelastic flows will produce the understanding necessary to tackle more realistic, and less tractable, viscoelastic problems.

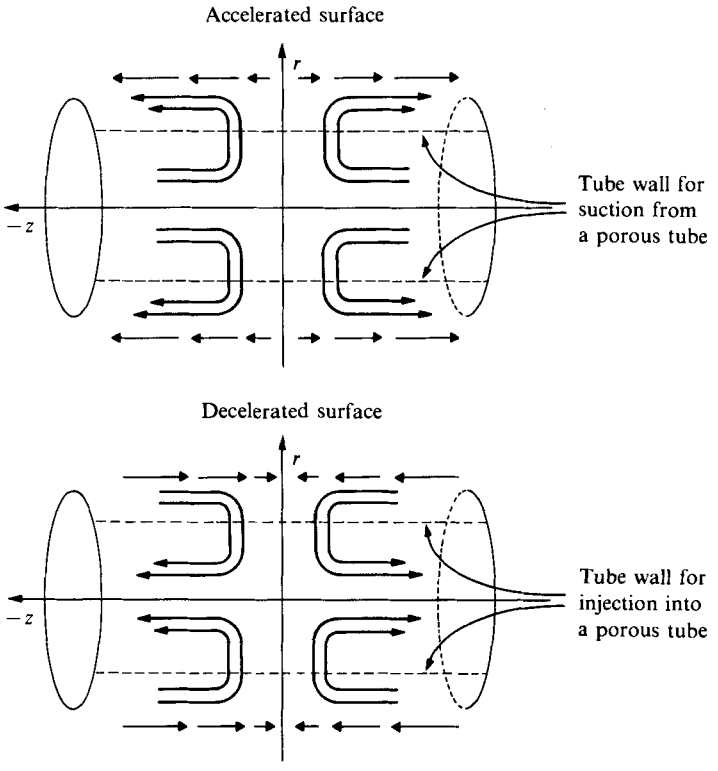

FIGURE 1. The accelerated-surface and porous-tube geometries.

2.1. *The upper-convected Maxwell equation*

To describe the viscoelasticity of the fluid, we use the upper-convected Maxwell equation,

$$De\,\overset{\nabla}{\boldsymbol{\tau}}+\boldsymbol{\tau}=2\boldsymbol{D}, \tag{5a}$$

where

$$\overset{\nabla}{\boldsymbol{\tau}}\equiv\dot{\boldsymbol{\tau}}-\boldsymbol{\nabla v}^{\mathrm{T}}\cdot\boldsymbol{\tau}-\boldsymbol{\tau}\cdot\boldsymbol{\nabla v} \tag{5b}$$

is the upper-convected time derivative and $\dot{\boldsymbol{\tau}}$ is the substantial time derivative. De, the dimensionless Deborah number, is the relaxation time of the material multiplied by a characteristic strain rate, in this case the velocity on the cylinder surface divided by the cylinder radius.

2.2. *Similarity solution*

The Maxwell equation is among the oldest and simplest constitutive equations of viscoelasticity; it exhibits some of the qualitative behaviour of real viscoelastic materials: stress relaxation, elastic recovery and normal stresses in simple shear. Its most important distinction with respect to the accelerated-surface problem, however, is that it is satisfied by the similarity solution

$$v_r=\frac{f(r)}{r},\quad v_z=\frac{-zf'(r)}{r}, \tag{6a, b}$$

$$-\tau_{rz}=k(r)\,z,\quad -\tau_{zz}=g(r)+\tfrac{1}{2}h(r)\,z^2, \tag{6c, d}$$

$$-\tau_{rr}=i(r),\quad -\tau_{\theta\theta}=j(r), \tag{6e, f}$$

$$p=p_0(r)+\tfrac{1}{2}p_1 z^2. \tag{6g}$$

The dependencies of velocity and stress on z exhibited by this similarity solution are also consistent with the momentum balance equation,

$$\nabla p - \nabla \cdot \boldsymbol{\tau} = \mathrm{Re}\, \boldsymbol{v} \cdot \nabla \boldsymbol{v}, \tag{7}$$

where Re is the Reynolds number, as well as the continuity equation for an incompressible fluid,

$$\nabla \cdot \boldsymbol{v} = 0. \tag{8}$$

Here the Reynolds number is the velocity of the accelerating surface times the cylinder radius, divided by the kinematic viscosity of the fluid. When the similarity forms, (6), are substituted into (5), (7) and (8), all z-dependencies cancel, and a set of seven ordinary differential equations are obtained that involve the seven r-dependent functions in (6). Of these seven equations, four must be solved as a coupled set (Menon *et al.* 1988), namely,

$$-p_1 = Re\left[\left(\frac{f'}{r}\right)^2 - \frac{f}{r}\left(\frac{f'}{r}\right)'\right] + \frac{1}{r}(rk)' + h, \tag{9}$$

$$f'' = \frac{f'}{r} + \frac{kr + De(fk' - f'k + kf/r)}{1 - De\, i}, \tag{10}$$

$$h' = -\frac{r}{f}\left\{\frac{h}{De} + 4k\left(\frac{f'}{r}\right)'\right\}, \tag{11}$$

$$i' = \frac{r}{f}\left\{2\left(\frac{f}{r}\right)'\left[i - \frac{1}{De}\right] - \frac{i}{De}\right\}. \tag{12}$$

2.3. *Boundary conditions*

We first present boundary conditions for suction from a porous tube, and then show the connection between this problem and that of an accelerated surface.

The boundary conditions for uniform suction from a porous tube, (2) and (6*a*) imply that

$$f(1) = 1. \tag{13}$$

A no-slip condition on the tube wall requires that

$$f'(1) = 0. \tag{14}$$

Slip at the wall may be allowed by using, instead of (14),

$$-\beta f'(1) = (1 - \beta)\, k(1), \tag{15}$$

where $\beta = 1$ corresponds to no-slip and $\beta = 0$ to perfect slip. Symmetry and continuity of v_r and v_z at the centreline give

$$f(0) = f'(0) = 0. \tag{16}$$

If i' and h' are bounded at $r = 0$, boundary conditions for the stress similarity functions at the centreline are obtained from the differential equations (10)–(12):

$$k(0) = h(0) = 0, \tag{17}$$

$$i(0) = \frac{-f''(0)}{1 - De f''(0)}. \tag{18}$$

2.4. *Rescaling*

We now have a complete set of boundary conditions for the differential equations (9)–(12). This problem can be solved with the aid of the rescaling technique introduced by Terrill (1964) for Newtonian flows and by Menon *et al.* (1988) for the flow of an upper-convected Maxwell fluid. We define new rescaled variables

$$\left.\begin{aligned} \xi &\equiv De^{\frac{1}{2}} p_1^{\frac{1}{2}} r, \quad p^* \equiv \frac{p_1}{|p_1|} \\ f(r) &\equiv De^{-2} |p_1|^{-1} F(\xi), \quad h(r) \equiv |p_1| H(\xi) \\ k(r) &\equiv De^{-\frac{1}{2}} p_1^{\frac{1}{2}} K(\xi), \quad i(r) \equiv De^{-1} I(\xi), \\ Re &= Re^* De^2 |p_1|. \end{aligned}\right\} \tag{19}$$

When these are substituted into (9)–(12), rescaled equations are obtained:

$$K' = -p^* - H - \frac{K}{\xi} - \frac{Re^*}{\xi^2}\left\{(F')^2 - F\left(F'' - \frac{F'}{\xi}\right)\right\}, \tag{20}$$

$$F''' = \frac{F'}{\xi} + \frac{-K\xi + F'K - F\left(K' + \dfrac{K}{\xi}\right)}{I-1}, \tag{21}$$

$$H' = \frac{1}{F}\left\{4K\left(\frac{F'}{\xi} - F''\right) - H\xi\right\}, \tag{22}$$

$$I' = \frac{1}{F}\left\{2(I-1)\left(F' - \frac{F}{\xi}\right) - I\xi\right\}. \tag{23}$$

The boundary conditions at the centreline become

$$F(0) = F'(0) = 0, \quad K(0) = H(0) = 0, \quad I(0) = \frac{-F''(0)}{1 - F''(0)}. \tag{24}$$

The no-slip boundary condition at the wall is satisfied by finding a rescaled position, ξ_s, at which $F' = 0$. Thus

$$F'(\xi_s) = 0. \tag{25}$$

Since at $\xi = \xi_s$, r and f must be unity,

$$1 = r_s = De^{-\frac{1}{2}} p_1^{-\frac{1}{2}} \xi_s, \tag{26}$$

$$1 = f(1) = De^{-2} |p_1|^{-1} F(\xi_s). \tag{27}$$

These two equations allow us to determine De and p_1:

$$De = \left|\frac{F(\xi_s)}{\xi_s^2}\right|; \quad p_1 = \frac{\xi_s^4}{F(\xi_s)}. \tag{28}$$

Thus the suction problem can be solved by choosing a value of $F''(0)$, and integrating out to ξ_s, the point at which the wall boundary conditions are satisfied. The values of ξ_s and $F(\xi_s)$ allow a determination of De and p_1.

The accelerated-surface problem can be solved by the same rescaling, except that the stopping condition is no longer $F' = 0$ but, from (2) and (6*a*), is

$$F(\xi_0) = 0, \tag{29}$$

where ξ_0 is the rescaled radial location of the accelerated surface. From (19), at the accelerated surface,

$$\left.\begin{aligned} 1 = f'(1) &= F'(\xi_0)\, De^{-\frac{3}{2}} p_1^{-\frac{1}{2}}, \\ 1 = r_0 &= De^{-\frac{1}{2}} p_1^{-\frac{1}{2}} \xi_0, \end{aligned}\right\} \tag{30}$$

giving

$$De = \left|\frac{F'(\xi_0)}{\xi_0}\right|; \quad |p_1| = \left|\frac{\xi_0^2}{F'(\xi_0)}\right|. \tag{31}$$

Now for the accelerated-surface problem, the boundary conditions on F and F', and the assumption that F has at least two derivatives, imply that F has an inflexion point where $F' = 0$, at some ξ between 0 and ξ_0. At the inflexion point, the no-slip boundary condition for the porous-tube problem is satisfied. Thus in the rescaled variables, a solution to the accelerated-surface problem contains on a smaller domain a solution to the suction problem.

The problem of injection of fluid into a porous tube also has solutions that are subsets of solutions to an accelerated-surface problem. For this case the relevant boundary conditions at the accelerating surface are

$$v_z(1) = -z; \quad v_r(1) = 0. \tag{32}$$

Thus the surface at $r = 1$ has a *negative* acceleration, that is a deceleration. In terms of the similarity functions, these boundary conditions lead to

$$f'(1) = -1; \quad f(1) = 0. \tag{33}$$

Thus suction into a porous tube is a subset of the accelerated surface flow, and injection is contained in the decelerated surface flow. We therefore concentrate hereinafter on the accelerated and decelerated surface flows.

3. Results

3.1. *Accelerated surface*

We solved this problem by a Runge–Kutta integration of the rescaled equations (20)–(23), starting from the centreline and integrating toward the accelerating surface. The step size typically used is $\Delta\xi = 5 \times 10^{-4}$, although smaller steps were used under conditions discussed shortly. As described in Menon *et al.* (1988) and Larson (1988), one must begin the integration with a perturbation expansion about $\xi = 0$, since F, which is in the denominator of (22) and (23), goes to zero as $\xi \to 0$. The perturbation expansions are given in the Appendix. Solving the equations for a range of $A \equiv F''(0)$ and Re^*, one can extract De, Re and p_1 from the stopping conditions, (31) and (19).

Figure 2 shows p_1 as a function of Re for De ranging from 0.05 to 1.2. At small Deborah number, $De = 0.05$, there is a turning point at $Re = 10.1$. Brady & Acrivos (1981) solved the accelerated-surface problem for Newtonian fluids, $De = 0$, and found a turning point at $Re = 10.25$. Thus our results are consistent with theirs. As De is increased, a second turning point initially at large negative p_1 approaches the first turning point, and by $De = 0.2$ the two have merged, leaving a monotonic relationship between Re and p_1.

For values of De of 0.2 and higher, inertia and elasticity act in opposition to each other in the sense that increasing inertia lowers p_1, while increasing elasticity raises it. As discussed below, the similarity solution disappears in the absence of elasticity when, at $Re = 10.25$, the inertia of the incoming fluid near the centreline overwhelms

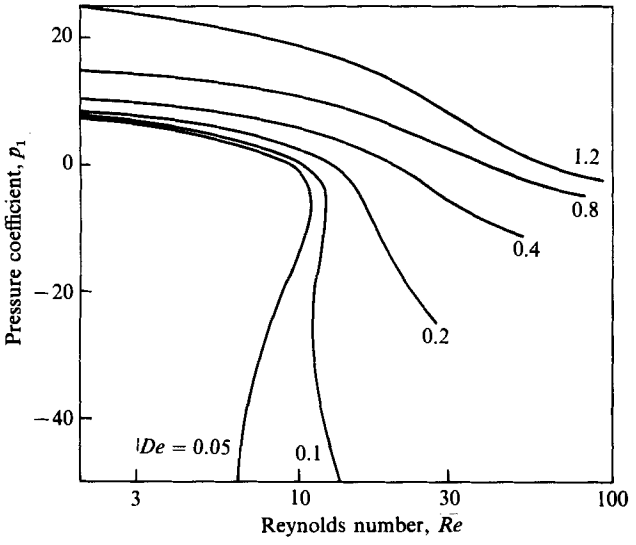

FIGURE 2. Solution families with inertia and elasticity for the accelerated surface.

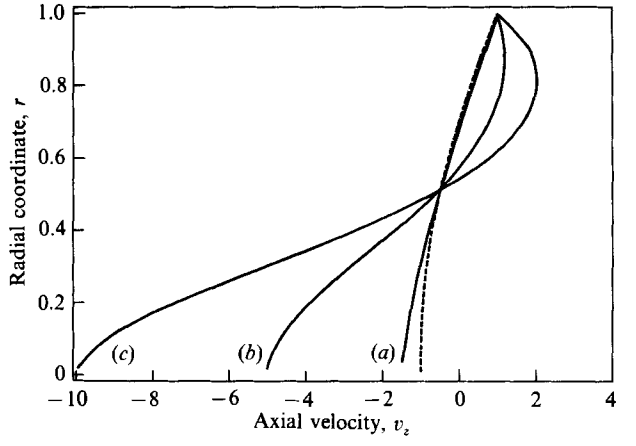

FIGURE 3. Axial velocity profiles for the accelerated surface at $De = 0.05$. The dashed line is the inertialess profile, with $De = 0$ or 0.05. (*a*) $Re = 10.0$ on the upper branch, (*b*) $Re = 7.4$ on the lower branch, (*c*) $Re = 5.7$ on the lower branch.

the braking action of viscosity. Elastic forces apparently assist the braking action of the viscous forces so that higher Reynolds numbers are attained before the similarity solution is lost.

Figure 3 shows the axial velocity, v_z, as a function of r, for $De = 0.05$. The values of Re for which profiles are plotted are 0, 10.0, which is near the turning point, and then 7.40 and 5.675 on the lower solution branch. The progression of change in the axial velocity profile, as one follows the solution family for $De = 0.05$, from $Re = 0$ to the turning point and along the lower solution branch, is very similar to that observed by Brady & Acrivos with no elasticity. Thus when $De = 0.05$, the influence of viscoelasticity on the velocity profile is small. At the turning point that occurs near $Re = 10$ when De is small, an inflexion point appears in the velocity profile. As Re decreases on the lower solution branch, there develop positive or outward velocities *greater* than that of the accelerated surface; towards the centre of the tube

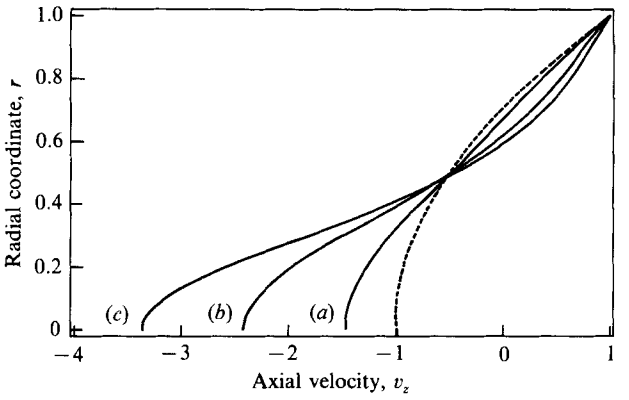

FIGURE 4. Axial velocity profiles for the accelerated surface at $De = 0.2$. The dashed line is the inertialess profile, with $De = 0$ or 0.2. (*a*) $Re = 14.91$, (*b*) $Re = 19.1$, (*c*) $Re = 28.5$.

the inward velocities become large. Because the inward velocities on the lower solution branch are large near the centreline, but velocity gradients are modest, inertial forces tend to dominate there, and one expects the pressure to be highest at the stagnation plane $z = 0$. This is consistent with the negative pressure gradient $p_1 < 0$ on the lower solution branch. Near the accelerated surface at low De on the lower solution branch, velocities are small but velocity gradients are steep and so viscous forces tend to dominate. Near the accelerated surface the negative pressure gradient is thus expected to produce a region with velocity profile concave towards the stagnation plane, as is indeed seen in figure 3.

In the absence of elasticity, the solutions with an inflexion point, that is those on the lower branch, are unstable. Between $Re = 10.25$ and $Re = 147$ there are no solutions for $De = 0$, and the solutions that appear for $Re > 147$ are unstable (Durlofsky & Brady 1984). Thus the turning point at $Re = 10.25$ marks the end of the stable *similarity solutions*, in the absence of elasticity. The reason for this loss of similarity solution, as Brady & Acrivos found, is that at $Re > 10.25$, the inward inertia of the returning fluid near the centreline cannot be overcome by fluid viscosity, and a 'collision region' develops near $z = 0$, where fluid moving inward from positive z collides with its mirror image moving inward from negative z. The collision region near $z = 0$ is a region of inviscid flow in which the similarity solution does not apply. By accounting for the inviscid collision region, Brady & Acrivos were able to compute numerical solutions for $Re > 10.25$ that were not of similarity form.

Figure 4 shows the axial velocity profiles for $De = 0.2$, as Re ranges from zero to 28.5. At $Re = 0$, the velocity profile is indistinguishable from that of a Newtonian non-elastic fluid. Thus elasticity, at a small magnitude corresponding to $De = 0.2$, has an insignificant effect when inertia is absent. But at increased Re, with De held fixed at 0.2, the presence of this low level of elasticity has a profound effect on the velocity profile. In contrast to the profiles for $De = 0.05$ shown in figure 3, the maximum positive axial velocity now always lies on the accelerated surface, and not inside the tube. The turning point has vanished. Thus *elastic forces, when coupled to inertial forces, have a profound influence not present when elastic forces of the same magnitude act alone.*

Axial velocity profiles for $De = 1.2$ are shown in figure 5. Here the profile is very different from Newtonian even at zero Reynolds number. The velocity profile is

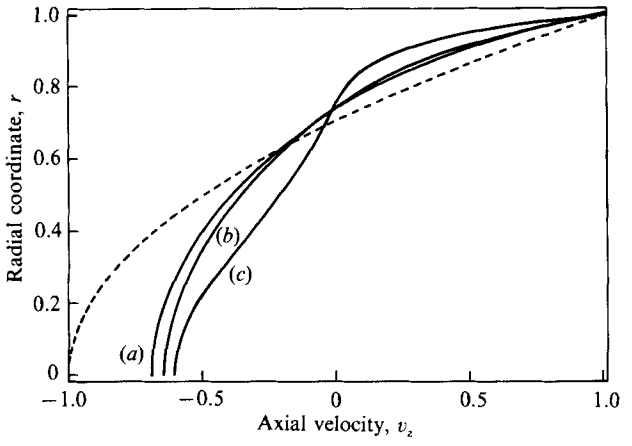

FIGURE 5. Axial velocity profiles for the accelerated surface at $De = 1.2$. The dashed line is the Newtonian, inertialess profile. (*a*) $Re = 0$, (*b*) $Re = 21.6$, (*c*) $Re = 92.4$.

steeper near the accelerated surface, and blunter near the centreline, when elasticity of this magnitude is present than when it is not. As inertia increases, the velocity on the centreline decreases. The opposite effect of inertia on the centreline velocity is seen at $De = 0.2$; see figure 4. Thus inertia and elasticity combine to produce complicated nonlinear non-monotonic results.

For the accelerated-surface problem, (20)–(23) can be solved for arbitrarily large Deborah numbers. This contrasts to the suction porous-tube problem, where a singularity appears at $De = 0.263$. This may seem paradoxical in the light of our earlier statement that the suction problem is contained within the accelerated-surface problem. The resolution of the paradox lies in noting that the definition of De for the suction problem differs from that of the accelerated-surface problem. For the suction problem, De is chosen so that v_r at the tube wall is unity; for the accelerated-surface problem it is chosen so that the velocity gradient, $\partial v_z/\partial z$, is unity at the accelerated surface. As De for the accelerated-surface problem becomes large, the velocity gradient concentrates itself near the accelerated surface, so that the velocities in the part of the domain corresponding to the porous tube become small. When the velocities in the part of the domain corresponding to the porous tube are rescaled so that $v_r = 1$ at the porous tube wall, the Deborah number is correspondingly reduced. Thus as De for the accelerated surface problem approaches infinity, De for suction approaches 0.263.

Although (19)–(23) can be solved for arbitrarily large De, without encountering any singularities, one of the similarity functions, $g(r)$, which is not solved as part of the coupled set, becomes singular at a Deborah number of $\frac{1}{2}$. $-g(r)$ is the z-independent part of the normal stress, τ_{zz}. $g(r)$ becomes singular because there is a uniaxial extension, $\partial v_z/\partial z = 1$; $\partial v_r/\partial r = -\frac{1}{2}$, on the accelerated surface. It is well known that for the upper-convected Maxwell equation τ_{zz} has a simple pole for a uniaxial extension of this magnitude at $De = \frac{1}{2}$. Uniaxial extensions at Deborah numbers greater than this are not considered physically meaningful. Thus the velocity profiles for the accelerated surface flow with $De > \frac{1}{2}$, such as those plotted in figure 5, have corresponding normal-stress components, τ_{zz}, that are unphysical. For suction from a porous tube, this pole lies outside the flow domain. Thus, the portion of each velocity profile in figure 5 that corresponds to suction from a porous tube,

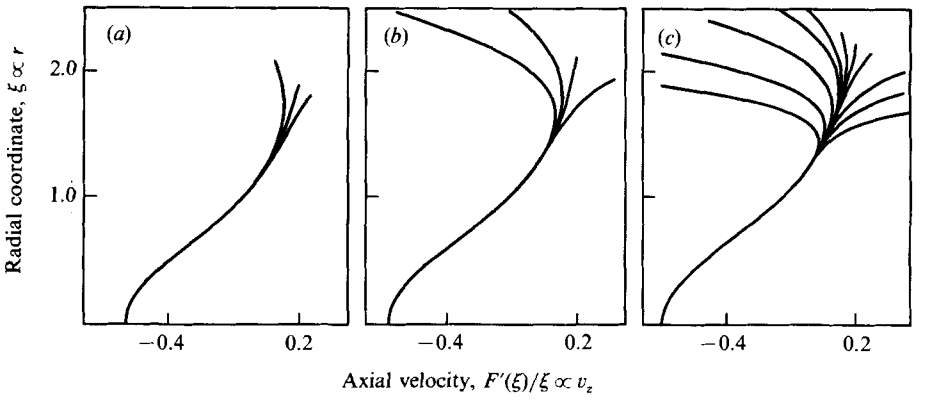

FIGURE 6. Rescaled solutions for an accelerated surface. (*a*) $A = 0.6$; clockwise: $Re^* = 29.7$, 30.0, 30.3. (*b*) $A = 0.67$; clockwise: $Re^* = 27.90$, 27.96, 27.99, 28.10. (*c*) $A = 0.70$; clockwise: $Re^* = 27.50$, 27.56, 27.58, 27.585, 27.586, 27.587, 27.588, 27.59, 27.60, 27.62, 27.70.

that is, the portion for which v_z is negative, may be considered a legitimate solution to the suction problem.

For each value of De, the solution family is traced in figure 2 up to a finite value of the Reynolds number. For example, for $De = 0.2$, the solution family is traced out to a terminal value of $Re = 28.5$. Solutions at higher values of Re were not obtained because, at this terminal value, there developed an extreme sensitivity to the rescaled Reynolds number, Re^*. Figure 6 shows how this sensitivity develops in the rescaled function $-F'(\xi)/\xi \propto v_z$ as $A \equiv F''(0)$ increases. There are two types of solution for $p_1 < 0$. One is a viscous-type solution with a single inflexion point that is similar to the zero-Deborah-number solutions for $p_1 < 0$. There is also a new elastic-type solution with two inflexion points. These two solution types diverge from each other near the second inflexion point of the elastic-type solution. The rate at which this divergence occurs as Re^* changes depends strongly on the value of A. At $A = 0.60$, the divergence shown in figure 6(*a*) is produced by changing Re^* from 29.7 to 30.3. When A is increased to 0.67, figure 6(*b*), a much larger divergence is produced by a smaller change in Re^*. When $A = 0.70$, figure 6(*c*), an even more dramatic divergence occurs when Re^* is changed slightly from 27.50 to 27.70. Obtaining these solutions required an especially accurate integration; the step size had to be reduced to 2.5×10^{-5}. When $A = 0.72$, a divergence as dramatic as that shown in figure 6(*c*) is obtained with a change in Re^* of only 10^{-5}. Furthermore when $A = 0.72$ even double-precision arithmetic (14 digits) is not adequate to avoid the influence of round off error in the integration. Since the moderate-De solutions ($De = 0.05$–0.40) in which we are specially interested lie in the transition region from viscous-type to elastic-type solutions, we cannot trace these solutions for values of A greater than 0.70.†

The elastic-type solutions have steep elastic boundary layers near the accelerating surface. This boundary layer is evident not only in the velocity profiles of figure 6 but more particularly in the gradients of the normal stress τ_{zz}. Figure 7 shows the rescaled normal-stress similarity function $-H(\xi)$, which is proportional to $\partial^2\tau_{zz}/\partial^2 z$ for $A = 0.70$ and Re^* values of 27.59–27.70. The left-most curve corresponds to a modest Deborah number of $De = 0.2$ and the right-most to a large Deborah number,

† Since the stopping point for the porous-tube problem, namely $F' = 0$, is achieved before this strong divergence, solution families for the suction porous-tube problem can be traced for $A > 0.70$.

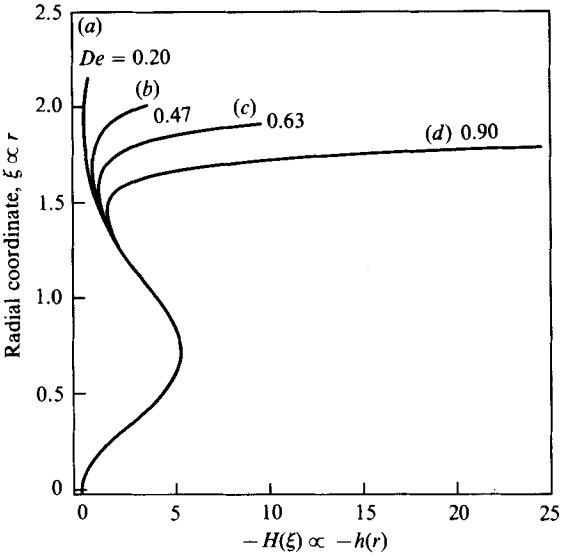

FIGURE 7. Similarity function $-H(\xi)$ for $A = 0.7$. (*a*) $De = 0.20$, $Re = 27$, $Re^* = 27.59$; (*b*) $De = 0.47$, $\mathrm{Re} = 51$, $Re^* = 27.60$; (*c*) $De = 0.63$, $Re = 64$, $Re^* = 27.62$; (*d*) $De = 0.90$, $Re = 80$, $Re^* = 27.70$.

$De = 0.9$. For the latter, a steep boundary layer in H appears near the accelerated cylinder. Since $-h \propto -H$ counterbalances the pressure coefficient p_1 in the momentum-balance equation (9), large normal stresses would be expected to make the pressure coefficient p_1 more positive. As De increases, the pressure coefficient does indeed increase, as can be seen in figure 2. In physical terms, near the accelerating surface the high-shear velocity gradients and the strong uniaxial extensional flow tend to stretch molecules, creating gradients in tensile force that increase the pressure gradient, offsetting the negative pressure gradients produced by inertia. The extreme confinement of the elastic boundary layer to the region near the accelerated surface at modest Deborah numbers and large Reynolds numbers is evidenced by the collapse of a whole family of solutions into a single curve in the core region near the centreline, as seen in figure 6(*c*). Because of this collapse, integration from the centreline outward becomes ill-posed.

Additional solution families were reported by Brady & Acrivos (1981) for the accelerated-surface problem for a non-elastic fluid at high Reynolds number ($Re \sim 10^3$). We found similar solution families for the Maxwell fluid but, since these solutions are unstable for Newtonian fluids, we do not consider them here. There may also be solutions that contain subregions of negative (or inward) radial flow; that is, there may be solutions with multiple stopping conditions. As discussed in the next section, integration is stable only in the direction of radial flow. Thus for the accelerated-surface problem, outward integration beyond the first stopping condition (at which $F = 0$) is unstable; only the first stopping condition can be found with the numerical technique developed here.

3.2. *Decelerated surface*

3.2.1. *Without inertia*

For the boundary conditions given in (4), the surface bounding the cylinder decelerates as it moves from large positive and negative z inward towards $z = 0$; see

figure 1. The decelerated-surface problem contains as a subset the problem of injection into a porous tube.

The decelerated-surface problem is more difficult to solve than the accelerated surface flow because the integration from the centreline outwards is unstable. The fluid's memory of its previous deformation history requires that the integration start at a position of zero radial velocity and *proceed in the direction of radial flow* (Larson 1988). For the decelerated surface, or the injection problem, this means the integration must start from the decelerated surface and go *towards the centreline.*

As was the case for the accelerated surface, since $F = 0$ at the starting point, the integration must be initiated with the first few terms of a perturbation expansion about the starting point, in this case about $\xi = \xi_0$. The Appendix contains the coefficients of the truncated perturbation expansion used here. Unlike the integration from the centreline, the integration from ξ_0 requires that one guess values of $F'(\xi_0)$ and $F''(\xi_0)$. If the guess is correct the integration will produce functions $F_{\text{int}}(\xi)$, $K_{\text{int}}(\xi)$, $H_{\text{int}}(\xi)$ and $I_{\text{int}}(\xi)$, that match the corresponding functions, $F_{\text{pert}}(\xi)$, $K_{\text{pert}}(\xi)$, $H_{\text{pert}}(\xi)$ and $I_{\text{pert}}(\xi)$ from the perturbation expansion near $\xi = 0$. Thus an iterative procedure for obtaining $F'(\xi_0)$ and $F''(\xi_0)$ is called for. We used a Newton–Raphson iteration; the details are in the Appendix.

Figure 8 shows the relationship between p_1 and De for the decelerated-surface problem. There is a simple pole at $De = 0.5$. This pole occurs because there is a biaxial extensional flow at the decelerated surface where $\partial v_z/\partial z = -1$ and $\partial v_r/\partial z = 2$. For a homogeneous biaxial extension of this magnitude, the upper-convected Maxwell equation has a simple pole at $De = \frac{1}{2}$. For the injection problem, which is a subset of the flow generated by the decelerated surface, there is a turning point at $De = 0.08$; see figure 9. The solutions along the upper solution branch in figure 9 are obtained as subsets of solutions found on the part of the curve in figure 8 labelled 'upper-branch solutions'. Thus going from a Deborah number defined from the porous-tube problem to one defined from the decelerated surface flow 'straightens out' the solution family. It is thus evident that the turning point for the injection problem is a manifestation of the biaxial pole of the Maxwell fluid which occurs in the larger domain of the decelerated surface flow. On the other hand the simple pole in De for the suction problem disappears on the larger domain of the accelerated surface flow.

3.2.2. *With inertia*

For the decelerated surface flow we could only consider the effects of small and moderate levels of inertia. This is because there is a limiting Reynolds number, which ranges from 8.7 when $De = 0.046$ to 6.9 when $De = 0.32$, beyond which our numerical scheme found no solutions. This limiting Reynolds number corresponds to a critical Re in the perturbation expansion about $\xi = 0$. In this perturbation expansion, all coefficients higher than zeroth order are polynomials in $P \equiv p^* + Re^* A^2$. For the decelerated surface only solutions with $p^* = -1$ were found; thus $P = 0$ when $Re^* = 1/A^2$. At this Re^*, terms of all order except zeroth in the perturbation expansion disappear. The remaining zeroth-order terms in the perturbation expansion correspond to a homogeneous extensional flow with homogeneous normal stresses and no shear stress. If the radius of convergence of the perturbation expansion about $\xi = 0$ is zero, then even when all derivatives of the velocities and stresses at the centreline correspond to a purely extensional flow, away from the centreline the flow need not be purely extensional. Nevertheless, no solutions were found at Reynolds numbers beyond the value at which $P = 0$.

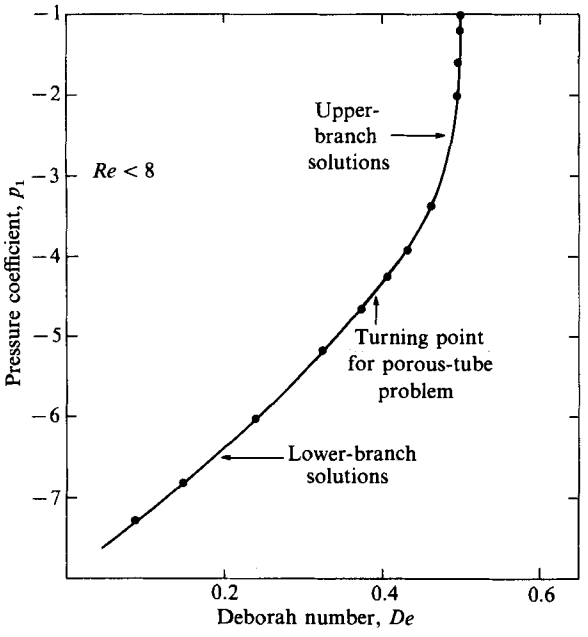

FIGURE 8. Solution family for the accelerated-surface problem, with $Re = 0$, or any Re less than the critical value.

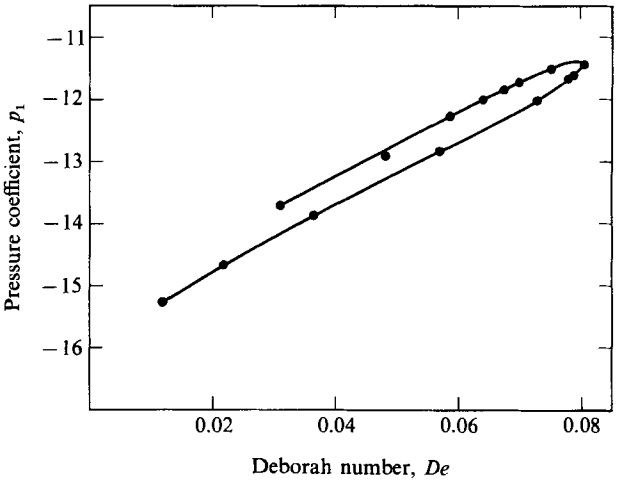

FIGURE 9. Solution family for the injection problem, generated as a subset of the accelerated-surface problem, with no inertia.

As De approaches zero, the critical Reynolds number presumably approaches infinity, since no critical Reynolds number exists for the non-elastic decelerated surface flow.

Inertia has virtually no effect on the relationship between p_1 and De shown in figure 8 for values of Re up to the largest attainable. Thus figure 8 holds for any Re less than about 8.

Figure 10 contains axial velocity profiles for the decelerated surface flow. Curve (*a*)

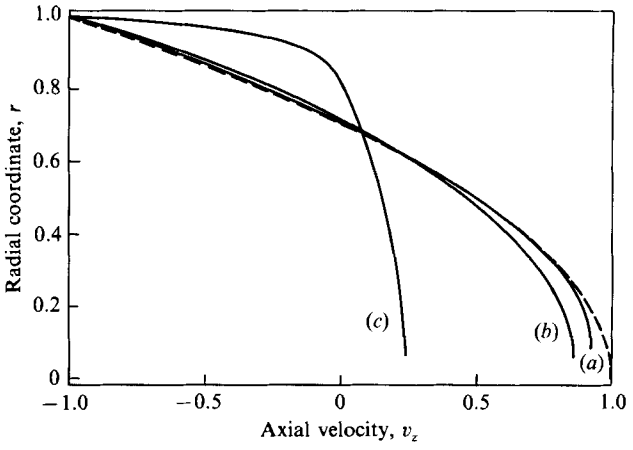

FIGURE 10. Axial velocity profiles for the accelerated surface. The dashed line is the inertialess Newtonian profile. (*a*) $De = 0.046$, $Re = 8.7$, (*b*) $De = 0.32$, $Re = 6.9$, (*c*) $De = 0.4994$, $Re = 0$.

corresponds to $De = 0.046$ with Re near its critical value of 8.7. The velocity profile for curve (*a*) is much like the Newtonian profile (dashed line), except near $r = 0$, where the inertial profile becomes blunt. The bluntness occurs because at the critical Re, all derivatives of v_z vanish on the centreline. The influence of elasticity on profile (*a*) is almost nil. Curve (*b*) corresponds to $De = 0.3204$, which is near the turning point for the injection problem, with $Re = 6.9$, very near its critical value for this De. Here there is again a blunting of the profile near $r = 0$, because of inertia. In addition there is a small change in shape over the whole range of r, which we found to be caused by elasticity. Curve (*c*) corresponds to $De = 0.4994$, near the pole, with $Re = 0$. At this De, elastic forces grossly distort the profile, pushing most of the velocity gradient to the decelerated surface. In the central part of the cylinder, where the velocity is positive, however, the profile is still very nearly parabolic. This part of the cylinder corresponds to the domain of the porous tube. When the velocity is rescaled to correspond to the injection problem in the porous tube, the nearly parabolic character of the velocity profile means that the velocity *in the porous tube* is nearly that of a Newtonian fluid. Thus the injection problem has nearly Newtonian velocities for all De; the decelerated-surface problem has a highly non-Newtonian velocity profile at Deborah numbers near the simple pole at $De = \frac{1}{2}$.

4. Summary

For similarity solutions of the accelerated surface flow, we have found that the turning point at $Re = 10.25$, found by Brady & Acrivos in the absence of elasticity, disappears as elasticity is introduced. Elasticity assists the viscous forces in balancing the inertia of the fluid as it approaches fluid coming from the opposite direction. An inviscid collision region is thus avoided, or at least delayed, by the introduction of elasticity. Elasticity and inertia couple in a complicated, nonlinear fashion. Small levels of elasticity, which scarcely affect the velocity profile in the absence of inertia, have a major effect when inertial forces are large. When elasticity is small or moderate, inertia acts to increase the centreline velocity; when elasticity is large, it decreases it. For each Deborah number, there is a maximum Reynolds

number beyond which the solution family cannot be traced because of extreme sensitivity of the solution to rescaled parameters, to the integration step size, and to roundoff error. This sensitivity emerges because at large Reynolds numbers and modest Deborah numbers the effect of elasticity is strongly confined to a boundary layer near the accelerating surface. Since the integration starts in the core region on the centreline where the level of elasticity has practically no influence, the integration technique becomes an ill-posed problem.

For the decelerated surface flow, there is a critical Reynolds number for each level of elasticity at which the axial velocity profile at the centreline becomes infinitely blunt. Solutions beyond this Reynolds number were not found. The effect of inertia at levels up to the critical Re is local; it blunts the velocity profile near the centreline. Elasticity serves to concentrate the velocity gradient into the region near the decelerated surface. A singularity induced by the extensional flow at the decelerated surface limits the range of elasticity to a maximum Deborah number of $\frac{1}{2}$.

Appendix

A.1. *Accelerated surface*

For the accelerated-surface problem, the Runge–Kutta integration was initiated by taking F, K, H and I from a perturbation expansion about $\xi = 0$:

$$\left.\begin{aligned} F &= \tfrac{1}{2}A\xi^2 + e\xi^4 + f_6\xi^6, \quad K = k_1\xi + k_3\xi^3, \\ H &= h_2\xi^2 + h_4\xi^4, \quad I = \frac{A}{A-1} + i_2\xi^2 + i_4\xi^4. \end{aligned}\right\} \tag{A 1}$$

The coefficients in the above expansions are obtained by putting (A 1) into the differential equations (20)–(23), and balancing terms of equal order in ξ. This gives

$$A \equiv F''(0), \quad P = p^* + Re^* A^2, \quad e = \frac{P(A-1)}{16}, \quad k_1 = -\tfrac{1}{2}P,$$

$$f_6 = \frac{Re^* P(A+1)(A-1)^2 A}{384}, \quad k_3 = \frac{-1}{4}\frac{A-1}{A+1}P^2 - Re^*(eA), \quad h_2 = \frac{(A-1)}{(A+1)}P^2, \quad i_2 = \tfrac{3}{8}P,$$

$$h_4 = \frac{P^2(A-1)^2}{2(2A+1)}\left[\frac{3}{4}\frac{P}{A+1} + \frac{Re^*(A+2)A}{4}\right], \quad i_4 = \frac{24e^2 + 10f_6}{(1+A)(A-1)}.$$

A.2. *Decelerated surface*

For the decelerated-surface problem, the integration starts at $\xi = \xi_0$, and proceeds towards $\xi = 0$. Since $F = 0$ at ξ_0, the integration must be initiated by a perturbation expansion about ξ_0:

$$\left.\begin{aligned} F &= f_1(\xi-\xi_0) + f_2(\xi-\xi_0)^2 + f_3(\xi-\xi_0)^3 + f_4(\xi-\xi_0)^4, \\ H &= h_0 + h_1(\xi-\xi_0) + h_2(\xi-\xi_0)^2, \quad I = i_0 + i_1(\xi-\xi_0) + i_2(\xi-\xi_0)^2, \\ & \qquad K = k_0 + k_1(\xi-\xi_0) + k_2(\xi-\xi_0)^2. \end{aligned}\right\} \tag{A 2}$$

The coefficients in the above are determined by matching terms of equal order in the differential equation. The coefficients are

$$
\left.\begin{aligned}
i_0 &= \frac{-\xi_0}{\xi_0-2f_1}+1, \quad i_1 = \frac{4f_1-4\xi_0 f_2}{(\xi_0-f_1)(\xi_0-2f_1)},\\
k_0 &= \frac{(2f_2\xi_0-f_1)(i_0-1)}{(f_1-\xi_0)\xi_0}, \quad h_0 = \frac{4k_0(f_1-2f_2\xi_0)}{\xi_0^2},\\
6\xi_0(i_0-1)f_3 &= k_1\xi_0(f_1-\xi_0)-(2f_2\xi_0-f_1)i_1+f_1\xi_0\left[p^*+h_0+\frac{Re^*f_1^2}{\xi_0^2}\right]\\
&\qquad +k_0(f_1+2f_2\xi_0-2\xi_0),\\
\xi_0^2 i_2 &= (i_0-1)(2f_2+6f_3\xi_0)+i_1(3f_2\xi_0-f_1-2\xi_0)-i_0,\\
k_1 &= \frac{-k_0}{\xi_0}-(h_0+p^*)-\frac{Re^*f_1^2}{\xi_0^2}, \quad h_1 = \frac{4k_1(f_1-2f_2\xi_0)-2h_0\xi_0-24k_0f_3\xi_0}{\xi_0(f_1+\xi_0)},\\
-2\xi_0 k_2 &= 2k_1+h_0+p^*+h_1\xi_0+\frac{Re^*}{\xi_0}2f_1f_2,\\
12(i_0-1)\xi_0 f_4 &= f_1(i_2+p^*+h_0+(h_1+k_2)\xi_0+k_1)+f_2[(p^*+h_0+2k_1)\xi_0+2k_0-2\xi_0 i_2]\\
&\qquad +3f_3[k_0\xi_0-2\xi_0 i_1-(i_0-1)]-k_0-2k_1\xi_0-k_2\xi_0^2+\frac{Re^*f_1^2}{\xi_0}\left(3f_2+\frac{2f_1}{\xi_0}\right),\\
\xi_0(2f_1+\xi_0)h_2 &= -h_0-h_1[f_1+2\xi_0(f_2+1)]-12k_0(f_3+4f_4\xi_0)\\
&\qquad -24k_1f_3\xi_0+4k_2(f_1-2f_2\xi_0).
\end{aligned}\right\}
\tag{A 3}
$$

$f_1 \equiv F'(\xi_0)$ and $f_2 \equiv F''(\xi_0)$ must be chosen so that after (20)–(23) are integrated from ξ_0 to the vicinity of $\xi = 0$, the functions $F_{\text{int}}(\xi)$, $K_{\text{int}}(\xi)$, $H_{\text{int}}(\xi)$ and $I_{\text{int}}(\xi)$ match the corresponding functions, $F_{\text{pert}}(\xi)$, $K_{\text{pert}}(\xi)$, $H_{\text{pert}}(\xi)$ and $I_{\text{pert}}(\xi)$ from the perturbation expansion near $\xi = 0$. We used a Newton–Raphson iteration, described as follows, to determine $F'(\xi_0)$ and $F''(\xi_0)$.

The perturbation expansions about $\xi = 0$ are determined once $A \equiv F''(0)$ is known. A can be obtained by taking $F_{\text{int}} = F_{\text{pert}}$ at some small value of ξ, say $\delta\xi$. (In this work, we take $\delta\xi = 0.05$; the sensitivity to this particular choice is small.) With A known, $K_{\text{pert}}(\delta\xi)$, $H_{\text{pert}}(\delta\xi)$ and $I_{\text{pert}}(\delta\xi)$ can be calculated and compared to $K_{\text{int}}(\delta\xi)$, $H_{\text{int}}(\delta\xi)$ and $I_{\text{int}}(\delta\xi)$. $F'(\xi_0)$ and $F''(\xi_0)$ must be varied until a match is obtained. The two unknown quantities, $F'(\xi_0)$ and $F''(\xi_0)$, can be determined by a match of only two of the three functions, K_{int}, H_{int} and I_{int} with their perturbation counterparts. In practice, if two of these functions match, the third also agrees closely with its counterpart. In the algorithm, we matched I and K, because the leading-order terms in the perturbation expansions for these functions are zeroth and first order in ξ respectively, compared to second order for H. The higher order in the perturbation parameter for H means that it is small near $\xi = 0$; thus it cannot be computed to as high as a relative accuracy near $\xi = 0$ as can I and K.

The following iterative procedure was used to find $F'(\xi_0)$ and $F''(\xi_0)$. Assume we have a solution, and we know $F'(\xi_0)$ and $F''(\xi_0)$ for a given ξ_0 and Re^*. Change one of the two parameters, ξ_0 or Re^* a small amount. Using the known $F'(\xi_0)$ and $F''(\xi_0)$ from the old solution, integrate the equations, and find the differences between $I_{\text{int}}(\delta\xi)$ and $I_{\text{pert}}(\delta\xi)$ and between $K_{\text{int}}(\delta\xi)$ and $K_{\text{pert}}(\delta\xi)$. Change $F'(\xi_0)$ a tiny amount, reintegrate the equations and find new differences between the I and K.

Change $F''(\xi_0)$ a tiny amount, and do the same thing. In this way a Jacobian matrix for the influence of $F'(\xi_0)$ and $F''(\xi_0)$ on the differences, $I_{\text{int}}(\delta\xi) - I_{\text{pert}}(\delta\xi)$, and $K_{\text{int}}(\delta\xi) - K_{\text{pert}}(\delta\xi)$ is obtained. With this Jacobian matrix, a Newton–Raphson procedure is used to obtain a new guess for $F'(\xi_0)$ and $F''(\xi_0)$. This procedure is then repeated until both relative differences fall to within a specified tolerance, usually about 3%.

REFERENCES

BRADY, J. F. & ACRIVOS, A. 1981 Steady flow in a channel or tube with an accelerating surface velocity. An exact solution to the Navier–Stokes equations with reverse flow. *J. Fluid Mech.* **112**, 127–150.

BRADY, J. F. & ACRIVOS, A. 1982 Closed-cavity laminar flows at moderate Reynolds numbers. *J. Fluid Mech.* **115**, 427–442.

DURLOFSKY, L. & BRADY, J. F. 1984 The spatial stability of a class of similarity solutions. *Phys. Fluids* **27**, 1068–1076.

LARSON, R. G. 1988 Analytic results for viscoelastic flow in a porous tube. *J. Non-Newtonian Fluid Mech.* (In the press.)

MENON, R. K., KIM-E, M. E., ARMSTRONG, R. C., BROWN, R. A. & BRADY, J. F. 1987 Injection and suction of an upper-convected Maxwell fluid through a porous-walled tube. *J. Non-Newtonian Fluid Mech.* (submitted.)

PHAN-THIEN, N. 1983*a* Coaxial-disk flow and flow about a rotating disk of a Maxwellian fluid. *J. Fluid Mech.* **128**, 427–442.

PHAN-THIEN, N. 1983*b* Coaxial-disk flow of an Oldroyd-B fluid: exact solution and stability. *J. Non-Newtonian Fluid Mech.* **13**, 325–340.

TERRILL, R. M. 1964 Laminar flow in a uniformly porous channel. *Aero. Quart.* **15**, 297–330.